

http://pubs.acs.org/journal/aesccq Article

Fluorescence Aerosol Flow Tube Spectroscopy to Detect Liquid— Liquid Phase Separation

Paul E. Ohno, Yiming Qin, Jianhuai Ye, Junfeng Wang, Allan K. Bertram, and Scot T. Martin*



Cite This: *ACS Earth Space Chem.* 2021, 5, 1223–1232



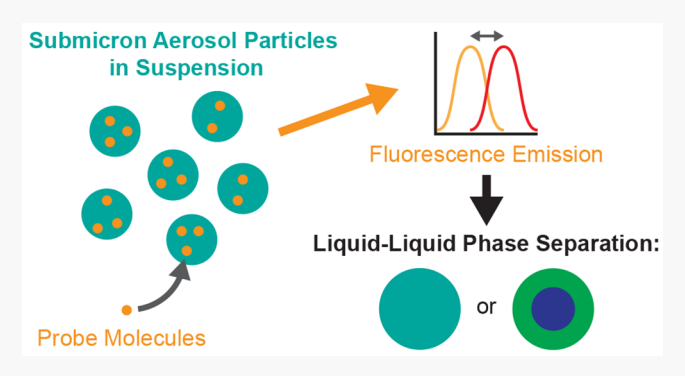
ACCESS

III Metrics & More

Article Recommendations

s Supporting Information

ABSTRACT: The phase behavior of atmospheric aerosol particles influences processes like gas-particle partitioning, solar light scattering, and cloud formation, ultimately affecting atmospheric air quality and climate. An important aspect of this phase behavior is whether an individual particle exists in a single homogeneous phase or undergoes liquid—liquid phase separation (LLPS). Herein, fluorescence aerosol flow tube (F-AFT) spectroscopy is developed to characterize LLPS in aerosolized submicron particles of 100—200 nm. A solvatochromic fluorescent probe molecule is incorporated into the particles. The link between its fluorescence emission and the local particle-phase chemical environment is used to determine the separation relative humidity (SRH) at which LLPS occurs. The LLPS behaviors of mixed organic/inorganic



particles composed of polyethylene glycol (PEG), ammonium sulfate (AS), and sodium chloride (NaCl) are characterized. PEG/AS particles undergo LLPS at SRH values that vary with PEG composition. By comparison, PEG/NaCl particles continue as a single homogeneous phase to the RH of NaCl crystallization. The SRH values for the submicron particles are lower by >5% RH than those reported in the literature for supermicron particles deposited to substrate surfaces. Possible reasons for the differences are discussed, including kinetic and thermodynamic effects of system size and foreign substrate as well as observation time in the experimental apparatus.

KEYWORDS: Liquid—liquid phase separation, aerosol particles, fluorescence, Nile Red, spectroscopy

1. INTRODUCTION

Aerosol particles are ubiquitous in the atmosphere and impact climate and air quality through a variety of mechanisms. ^{1,2} They directly scatter and absorb solar radiation, serve as cloud condensation nuclei, and threaten human health when inhaled. ^{3–5} The extent of these effects is controlled by the physical and optical properties of the particles, which are ultimately determined by the physical processes and chemical reactions that control particle formation, growth, and transformation. ^{6,7} Liquid—liquid phase separation (LLPS) is one such process of recent scientific interest that has important effects on particle properties yet remains incompletely understood. ^{8–13}

Deliquescence, efflorescence, freezing, and melting are processes well documented for atmospheric particles. ¹⁴ Deliquescence describes the transition of a solid into a saturated aqueous solution by water uptake from the surrounding atmosphere. Efflorescence describes the reverse transition of a saturated aqueous solution into a solid by water evaporation to the atmosphere. Both processes are driven by atmospheric relative humidity (RH). Gas-particle exchange ensures that the water activity in a particle equals RH/100, possibly modified by a Kelvin effect, when the particle and surrounding atmosphere

are in thermodynamic equilibrium with one another.¹⁵ Atmospheric temperature drives additional solid/liquid transitions through freezing and melting.¹⁴ These four phase transitions foresee atmospheric scenarios of particles that are (i) a single solid or mix of solids, (ii) one or more solids in contact with aqueous solution, or (iii) a single homogeneous aqueous solution.¹⁶

Evidence that LLPS occurs in atmospheric particles brings forward additional atmospheric scenarios. 8-10,12,13,17-26 Mixed organic/inorganic aerosol particles are common in the Earth's atmosphere. 3,5 In the atmospheric context, LLPS describes an event in which a single aqueous solution of mixed organic/inorganic composition spontaneously separates into two liquids. This demixing occurs below a threshold separation RH (SRH). Experimental observations 18 and theory 27 typically show that one phase is an aqueous salt solution from which organic

Special Issue: Mario Molina Memorial

Received: March 6, 2021 Revised: April 26, 2021 Accepted: April 27, 2021 Published: May 6, 2021





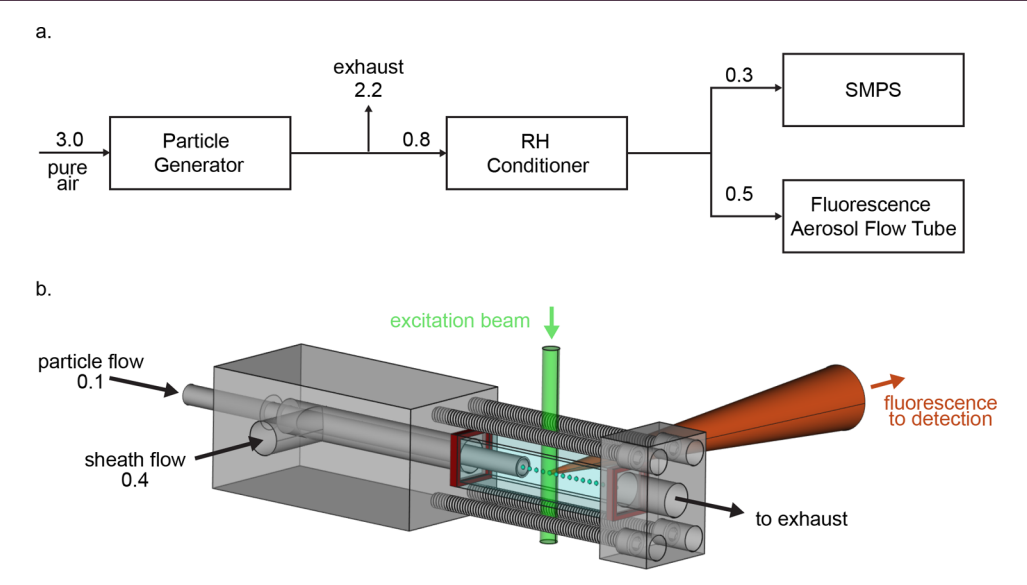


Figure 1. (a) Diagram of the experimental apparatus used to produce an aerosol suspension, condition its relative humidity (RH), and measure its fluorescence. The arrows show the direction of aerosol flow. The numbers over arrows represent flow rates (Lpm). The number-diameter distribution of the aerosol particles was measured by a scanning mobility particle sizer (SMPS). (b) Diagram of the optical configuration of the fluorescence aerosol flow tube (F-AFT).

molecules are largely excluded. The other phase is rich in organic molecules, and salt ions are largely excluded. The water content of the organic-rich phase depends on the hygroscopicity of the organic material and the prevailing RH, and in some cases water is largely excluded as well. LLPS particles can exhibit different morphologies, such as core—shell or partially engulfed. The outer layer is typically the organic-rich phase, and in a core—shell particle the inner aqueous salt core is completely covered by the organic-rich shell. For a partially engulfed particle, the aqueous phase is partially exposed to the surrounding atmosphere.

The presence or absence of LLPS can affect many particle properties. LLPS modifies the chemical composition of the surface region of a particle, thereby changing the rates of heterogeneous reactions. ^{28,29} LLPS can lead to changes in the optical properties of particles and thus alter light scattering properties. ^{30–32} LLPS can alter gas-particle partitioning by influencing the chemical potential of dissolved species. ³³ Such changes can have further follow-on atmospheric effects. In this regard, inclusion of LLPS in two different air quality models decreased the simulated mass concentrations of atmospheric particulate matter by 10–70% under some conditions. ^{27,34} LLPS can also alter the ability of particles to act as cloud condensation nuclei. ^{35–39}

Hindering advances in the understanding and quantification of LLPS is the challenge of directly probing the phase state of atmospheric aerosol particles. These particles occur in the atmosphere at typical number densities of 10³ to 10⁴ cm⁻³ in a submicron diameter regime. This challenging combination of low density and small diameter has led many laboratory investigations to study particles deposited on substrates rather than in aerosol form. Single suspended particles levitated in particle traps have also been studied. In both of these configurations, however, the composition of a captured particle can differ substantially from that of the parent aerosol particle. This difference can arise because of the dynamic gasparticle exchange of semivolatile compounds, often organic molecules, that affect particle composition. Continuous exposure of captured particles to a gas stream containing semivolatile compounds can alleviate this issue, 46,47 although

accurately mimicking the complex and dynamic mixture of gases that exist in the atmosphere is challenging.

Particles in capture methods are also typically supermicron. These particles can differ in volume by a factor of 10⁶ and surface area by a factor of 10⁴ compared to the submicron particles that dominate the atmosphere. The incompletely understood scaling effects of volume and surface area on LLPS and SRH increase the challenge of extrapolating results among size regimes. Cryogenic transmission electron microscopy (cryo-TEM) has been applied to the study of LLPS in submicron particles, and a size dependence in LLPS was observed. 24,26,48 Larger particles phase separated while smaller particles remained homogeneous. This transition occurred between 30 and 200 nm for different particle systems. The cryo-TEM technique was further extended by coupling to an RH-adjusted flow tube to flash-freeze particles, and these particles were collected, preserved, and imaged in the cryo-TEM.⁴⁹ Differences across a series of images allowed a determination of SRH. For some mixed organic/inorganic particles, the SRH of the submicron particles was lower by up to 15% RH than their supermicron counterparts.

These challenges and findings described above motivate the development of complementary techniques that can directly probe the phase state of submicron aerosol particles in suspension with minimal sample preparation or perturbation. The study herein introduces and validates such a technique based on fluorescence aerosol flow tube (F-AFT) spectroscopy. The F-AFT is applied to determine the SRH values for several different aerosol systems. The technique is enabled by the sensitivity of fluorescence and the link between the fluorescence emission of solvatochromic probe molecules and local physicochemical properties.⁵⁰ A fluorescent probe molecule is incorporated at a low concentration into the particles, and its fluorescence emission is used to indicate the particle phase state. Mixed organic/inorganic particles of polyethylene glycol (PEG), ammonium sulfate, and sodium chloride are studied. Ammonium sulfate and sodium chloride represent two of the most abundant inorganic constituents in atmospheric aerosol particles.14 PEG, although not abundant in atmospheric particles itself, contains many of the chemical functional groups that are commonly found in ambient aerosol particles, and as such, it is used as a model system for atmospheric organic compounds. 10,23,51,52

2. EXPERIMENTAL SECTION

Figure 1 shows a schematic diagram of the experimental apparatus used to produce the submicron aerosol particles, condition the relative humidity of the aerosol flow, measure the fluorescence of the aerosol particles in a flow tube geometry, and characterize the number-diameter distribution of the aerosol particles.

2.1. Particle Production and RH Conditioning. The aerosol particles were produced by atomization of aqueous solutions of the particle-phase components. For the organic component, solutions of polyethylene glycol (PEG) were prepared at a concentration of 0.2 g L-1 (Millipore water, resistivity of 18.2 M Ω cm). PEG200 and PEG300 were used (Sigma-Aldrich, P/N 91462 and P/N P3015). They have average molecular weights of 200 and 300 g mol⁻¹, respectively. For the inorganic component, solutions of ammonium sulfate $((NH_4)_2SO_4$, hereafter, "AS"; purity of $\geq 99.0\%$; Sigma-Aldrich P/N A4915) and sodium chloride (NaCl; purity of \geq 99.0%; VWR P/N BDH9286) were prepared at a concentration of 0.1 g L⁻¹. For mixed particles, two-component solutions were prepared of 0.2 g L-1 of PEG200 or PEG300 as component one and 0.1 g L⁻¹ of AS or NaCl as component two. The solvatochromic fluorescent probe molecule Nile Red (Sigma-Aldrich, P/N 72485) was mixed at 0.1% (w/w) with the PEG prior to preparing the aqueous solutions. The concentration of Nile Red was thus 0.2 mg L^{-1} in the aqueous solutions used for atomization. In the analysis, the dry composition of the aerosol particles was taken as the same as the dry composition of the atomization solution. In principle, semivolatility of any of the constituents could lead to a deviation in composition and a change in the organic-to-inorganic ratio. However, in the present study, none of the particle constituents except water was

For aerosol production, a syringe pump (New Era Pump Systems, P/N NE-1000) fed the aqueous solutions into an atomizer (TSI, P/N 3076). The liquid flow rate was 0.75 mL min $^{-1}$. The atomizer was operated at 170 kPa (24 PSI) of air flow (AADCO Pure Air Generator, P/N 737-12A). The atomizer produced an outflow of 3.0 Lpm of aerosol particles, of which 2.2 Lpm was sent to exhaust and 0.8 Lpm was used in the downstream experimental apparatus (Figure 1a). The aerosol flow exiting the atomizer had an RH of >95% so that the AS and NaCl particles were in aqueous form prior to the entry of the aerosol flow into the downstream RH conditioner. In some experiments, the conditioner reduced the relative humidity below the respective efflorescence RH (ERH) values of 35% and 45% for AS and NaCl, and solids could form. 14 The temperature of the experiments was 20 \pm 1 $^{\circ}$ C.

The RH conditioner consisted of parallel flow through 200 Nafion tubes (Perma Pure, P/N PD-200T-24MPS, 60 cm length, 0.76 mm tube inner diameter). The Nafion membrane of the tube walls allowed RH equilibration between the internal aerosol flow and the external counterpropagating sheath flow. The RH of the sheath flow was adjusted by mixing a controlled ratio of dry air and wet air within a proportional-integral-derivative (PID) control loop in conjunction with an RH sensor at the outflow of the RH conditioner (Omega, RH-USB). The stated accuracy of the RH sensor was ±3% RH. The sensor was further calibrated using saturated salt solutions, and its

repeatability was $\pm 1\%$ RH. The wet air was produced by bubbling through Millipore water. For a length of 60 cm and a flow rate of 0.8 Lpm, the residence time of the aerosol flow inside the RH conditioner was 4 s. In a typical sequence of experiments, the aerosol RH was adjusted stepwise from 30 to 90% RH. After RH conditioning, the aerosol flow of 0.8 Lpm was split so that 0.5 Lpm passed into the fluorescence aerosol flow tube (section 2.2) and 0.3 Lpm passed into a scanning mobility particle sizer (SMPS) (section 2.3). ⁵³

2.2. Fluorescence Aerosol Flow Tube. A diagram of the fluorescence aerosol flow tube is shown in Figure 1b. A quartz cuvette (10 mm × 10 mm × 45 mm; FireFly Sci., Staten Island, NY, P/N 3FT) was held in a machined aluminum housing. The cuvette and housing were sealed with custom laser-cut silicone gaskets (GraVy Laboratories, Somerville, MA).

The aerosol flow of 0.5 Lpm that passed into the F-AFT was divided, and 0.1 Lpm was used for the sample flow. The remaining flow of 0.4 Lpm passed through a HEPA filter (Whatman, P/N 6702-7500) to remove the aerosol particles, and this flow was used downstream as a sheath flow. The sample flow of 0.1 Lpm entered into grounded conductive silicone tubing and further through a stainless-steel tube (4.8 mm o.d., 4 mm i.d.). The sheath flow passed around the outside of the tube in the same flow direction. The exit of the tube was positioned at the center of the cuvette cross section, and the two flows combined with little lateral mixing. In this way, the sample flow continued along the central axis of the cuvette and entered the optical excitation volume (see below) while the sheath encased it annularly. The linear velocity of 10 cm s⁻¹ for the sample flow corresponded to a residence time of 0.4 s in the cuvette. The linear velocity of the sheath flow was 8 cm s^{-1} , corresponding to approximate isokinetic sampling and little shearing force between the two flows. The sheath flow prevented deposition of particles onto the cuvette walls, thus obviating an otherwise possible contribution to the detected fluorescence. The Reynolds numbers of approximately 30 for each flow indicated a laminar regime and little lateral mixing, as supported by visual containment of the particles along the central axis of the cuvette when profiled by a laser. To obtain a particle-free excitation volume for background fluorescence spectra, a valve placed inline with the sample flow was actuated to redirect the entire 0.5 Lpm through the HEPA filter, resulting in all sheath flow and no

The optical excitation volume where the pump laser beam and the particle flow overlapped occurred in the center of the cuvette, approximately 5 mm beyond the stainless-steel tubing. The aerosol particles in the excitation volume (approximately 6 mm³) were exposed to 100 mW of 532 nm light from a continuous wave diode pumped solid state laser (Laserglow Technologies, Toronto, Canada, P/N R531001FX). The beam width $(1/e^2$, containing 86.5% of the intensity of a Gaussian beam) was 2 mm, and the beam was not focused. The fluorescence emitted from the excitation volume was sampled at the angular cross product to the directions of the particle flow and the excitation beam. An achromatic doublet lens (focal length of 50 mm, diameter of 30 mm, Thorlabs, P/N AC300-050-A) focused the fluorescence onto the entrance slit of a scanning monochromator (Spectral Products, Putnam, CT, P/ N CM110). The monochromator grating had 1200 groove mm⁻¹ (P/N AG1200-00500-303), corresponding to a nominal resolution of <4 nm for a 0.6 mm slit width. The light exiting the monochromator was incident upon a photon counting head (Hamamatsu, P/N H8259-01) connected to a counting board

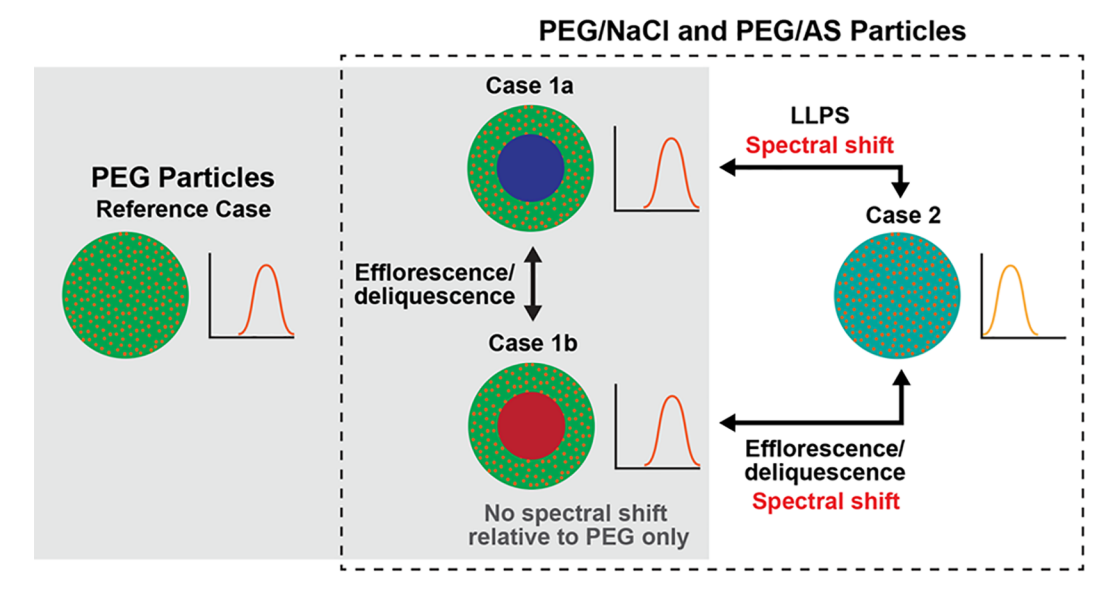


Figure 2. Schematic depiction of spectral shifts associated with particle morphologies and phase separation. See further in the main text. Red and blue coloring denote solid and aqueous inorganic cores, respectively.

(Parallax, P/N P8X32A). The counting board, monochromator, and laser were computer-interfaced for control. Individual fluorescence spectra were acquired with a step size of 2 nm from 528 to 726 nm, 4 s per point, for a total scan time of <10 min. As part of the data analysis, the spectra acquired for background conditions in the absence of aerosol particles were subtracted from the sample spectra.

Particle mass concentrations of 100 μ g m⁻³ were required to acquire fluorescence spectra of adequate signal-to-noise. For these mass concentrations, typical photon count rates varied from 100 to 1000 counts s⁻¹ depending on wavelength and RH. By comparison, spectra for control experiments using PEG300 particles without Nile Red as well as control experiments using particle-free background conditions had electronic noise (i.e., dark counts) of 40 counts s⁻¹. The standard deviation of photon shot noise corresponds to the square root of counts s⁻¹, meaning that for 100 counts s⁻¹ a shot noise of 10 counts s⁻¹ corresponds to fluctuations of the signal of 10%. Photon shot noise was the dominant source of noise in the fluorescence spectra rather than any other instabilities in the apparatus. For each sample condition, at least three individual sequential fluorescence scans were recorded to verify that the spectral variability did not exceed what could be explained by shot noise.

2.3. Size Distribution of the Particle Population. The SMPS consisted of a TSI differential mobility analyzer (DMA, model 3081) and an ultrafine condensation particle counter (CPC, model 3776).⁵³ The CPC was operated at a flow rate of 0.3 Lpm. The DMA was operated similarly to previously reported,⁵⁴ and the terminology herein follows that publication. The sheath and excess flows of the DMA were 3.0 Lpm. The RH of the sheath flow was matched to the RH of the aerosol flow by varying the ratio of dry air and wet air in the sheath flow. An RH sensor (Omega, RH-USB) monitored the RH of the sheath flow. For an aerosol RH above 80%, the RH of the sheath flow was nonetheless maintained at 80% to prevent water condensation inside the DMA or CPC. The flow rate of the sheath flow was controlled using a PID controller (Omega, P/N CNi16D52-C24-DC) connected to a sealed compressive blower (Ametek, Berwyn, PA, P/N SE12RE21SA) and a laminar flow element (Furness Controls, U.K., P/N FCO96E). A stainless-steel,

finned-tube heat exchanger (Lytron, P/N 4105G1SB) prevented any blower-induced temperature rise. The flow rate of the DMA excess flow was controlled by a mass flow controller (Alicat, P/N MC-10 SLPM-D) connected between the excess flow port and vacuum. Flows were calibrated regularly using a bubble flowmeter (Sensidyne, Gillibrator-2).

3. RESULTS AND DISCUSSION

3.1. Fluorescence Spectra to Indicate LLPS. Nile Red (NR), widely used as a hydrophobic fluorescent stain for lipid droplets and other hydrophobic cellular inclusions, ⁵⁵ partitions strongly from water into hydrophobic solvents. ⁵⁶ Thus, it preferentially segregates into organic domains when they coexist alongside an aqueous phase, as occurs in LLPS. Furthermore, NR is both photostable and can be excited at 532 nm. This long wavelength is advantageous for avoiding fluorescence interference from many organic molecules of interest in the context of atmospheric chemistry. As an example, the fluorescence of secondary organic material produced by the oxidation of α -pinene and limonene peaks upon excitation between 300 and 450 nm. ⁵⁷ NR also has a high fluorescence yield in hydrophobic environments. As such, particle-phase concentrations can be sufficiently low that thermodynamic properties relevant to LLPS should be unaffected.

As a solvatochromic probe molecule, the fluorescence emission of NR depends strongly on its local chemical environment. The wavelength $\lambda_{\rm max}$ of maximum emission and its intensity can both change. These changes can be used to indicate whether the probe molecule is in a predominantly organic phase, meaning a two-phase LLPS particle, or alternatively in a phase containing a mixture of organic molecules, inorganic ions, and water, meaning a single-phase particle. The relationship between spectral shift and particle phase is depicted conceptually in Figure 2. The reference case is a pure organic particle as a single phase. The associated NR fluorescence spectrum is depicted schematically in the figure. Mixed organic/inorganic particles are depicted in the figure as (case 1a) an organic outer layer with an aqueous inorganic core, (case 1b) an organic outer layer with a solid inorganic core, and

(case 2) a completely mixed particle. The NR fluorescence spectra for these cases are shown schematically in Figure 2, and shifts in the NR fluorescence spectra indicate transitions between LLPS (i.e., case 1a) and a single phase (i.e., case 2). The spectra of cases 1a and 1b are similar to that of the reference cases whereas the spectrum of case 2 substantially differs.

For case 2, the addition of inorganic ions and associated water can influence fluorescence in at least two different ways. In one regime, NR molecules remain as monomers dissolved in the solvent. As RH around the particle increases, the water content of the particle increases, implying that the solvent around a single NR molecule grows increasingly polar.⁵⁸ As a result, the fluorescence emission decreases in intensity and red shifts for this increasingly polar environment. In another regime, NR molecules begin to aggregate.⁵⁹ Aggregation is favorable in a strongly polar yet still nondilute environment, such as in particles of high water content above a threshold RH. Aggregates have modified electronic energy levels, and the fluorescence behavior thus changes. 60 Dimer formation leads to blueshifting. 61,62 The magnitude of the blue shift depends on the concentrations and types of dimers and monomers and in some cases could be as large as 50 nm. 61 Thus, in the current experiments, an increase from low to intermediate RH can correspond to a regime of red shifting, which is then followed above a threshold RH by a regime of blue shifting. As an example from Dutta et al.,⁶³ increasing the water mole fraction in binary methanol/water mixtures causes the emission of NR to initially red shift, attributed to increasing polarity, before reversing the trend at high water mole fractions and blue-shifting, attributed to the formation of aggregates. LLPS can thus plausibly cause a spectral shift in either direction relative to the reference spectrum depending on the position of the SRH relative to the threshold RH between polarity/aggregation dominance. For this reason, the interpretation of the spectral changes herein focuses on the presence of a spectral shift rather than its direction relative to the reference spectrum.

3.2. Aerosol Fluorescence Emission in Flow-Tube **Configuration.** 3.2.1. Pure PEG300 Aerosol Particles. Pure PEG300 aerosol particles represent the reference case depicted in Figure 2. Aerosol fluorescence spectra are shown in Figure 3 for particles at 50% RH having mass ratios of 0, 0.01%, and 0.1% between NR and PEG300. NR concentrations are given as the ratio of the mass of NR to the mass of PEG because this value remains invariant with RH. Furthermore, because NR partitions strongly to the organic phase, the stated mass ratio is representative of the NR concentration in its local environment for organic-only reference particles as well as for phase-separated mixed particles (assuming negligible hygroscopicity of the organic phase). The spectra were recorded using the F-AFT apparatus of Figure 1. As expected, pure PEG300 particles did not fluoresce in the absence of the probe. For increasing NR concentrations, the fluorescence intensity increased while λ_{\max} at 636 nm did not shift appreciably. The increase in the probe concentration by a factor of 10 did not lead to a full factor of 10 increase in the fluorescence intensity. The signal nonlinearity could be caused in part by optical saturation and in part by NR aggregation.59

Fluorescence spectra of NR in PEG300 aerosol particles are shown in Figure 4a from 30% to 90% RH at a mass ratio of 0.1% between NR and PEG300. PEG300 aerosol particles undergo continuous hygroscopic growth with increasing RH. From 30% to 90% RH, the diameter growth factor of the hydrated particle relative to the dry particle increases from 1.01 to 1.28. Figure

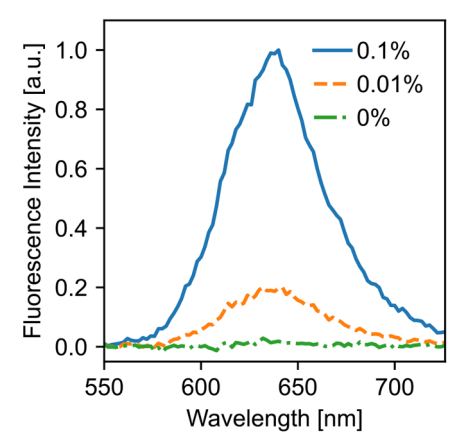


Figure 3. Aerosol fluorescence spectra for variable mass concentration of Nile Red in PEG300. Each spectrum is normalized such that the experimental condition producing the largest signal intensity has a fluorescence intensity of 1 au. Results are for an aerosol suspension of submicron particles at 50% RH. The legend indicates the concentration, which is expressed as the ratio of the mass of Nile Red to the mass of PEG300. At 50% RH, there is additionally an estimated 12% (w/w) of water in PEG300. 51

4a shows that both the fluorescence intensity and λ_{max} varied with RH. The intensity decreased by 10-fold from 30 to 90% RH, and λ_{max} red-shifted by 9 nm from 634 to 643 nm. These λ_{max} values lay between those of NR in pure PEG300 (630 nm) and pure water (652 nm) (Figure S1, Supporting Information).

The decrease in intensity and the associated red shift in response to the greater water content at increasing RH, subsequently followed by an absence of further change or a blue shift at even higher RH, are consistent with the explanation of section 3.1. Below 75% RH, increasing local polarity dominated the effect on NR fluorescence, as indicated by the linear relationship of water mass fraction with both fluorescence intensity and $\lambda_{\rm max}$ (Figure S2). These linear relationships, however, did not continue at higher RH, as explained by the occurrence of aggregation.

The results for NR fluorescence in pure PEG300 aerosol particles, as plotted in Figures 3 and 4a, serve as the reference conditions for understanding changes in the fluorescence behavior of mixed particles (sections 3.2.2 and 3.2.3).

3.2.2. Mixed PEG300/AS Aerosol Particles. Mixed PEG300/ AS aerosol particles represent cases 1a, 1b, and 2 depicted in Figure 2. The fluorescence spectra of NR in the mixed particles are plotted in Figure 4b from 30% to 90% RH. The general trend of a decrease in fluorescence intensity with RH is similar to that of the reference case (i.e., Figure 4a compared to Figure 4b). Important differences, however, are revealed by taking difference plots (Figure 4c). For 70% RH and below, there are no substantial differences between the spectra of the mixed particles and the reference spectra. In contrast, for 80% RH and above, strong differences are apparent (Figure 4c). The observations are further explored by plotting λ_{max} of the two sets of spectra as a function of RH (Figure 5a). The λ_{max} value of an individual spectrum is obtained by a Gaussian fit across the central band. The dashed line in Figure 5a delineates a regime at low RH for which λ_{max} converges with the reference spectra from a regime at high RH for which λ_{max} diverges.

Phase-separated morphologies at low RH and single-phase morphologies at high RH can explain the delineation into these two RH regimes. For 75% RH and below, the spectra indicate

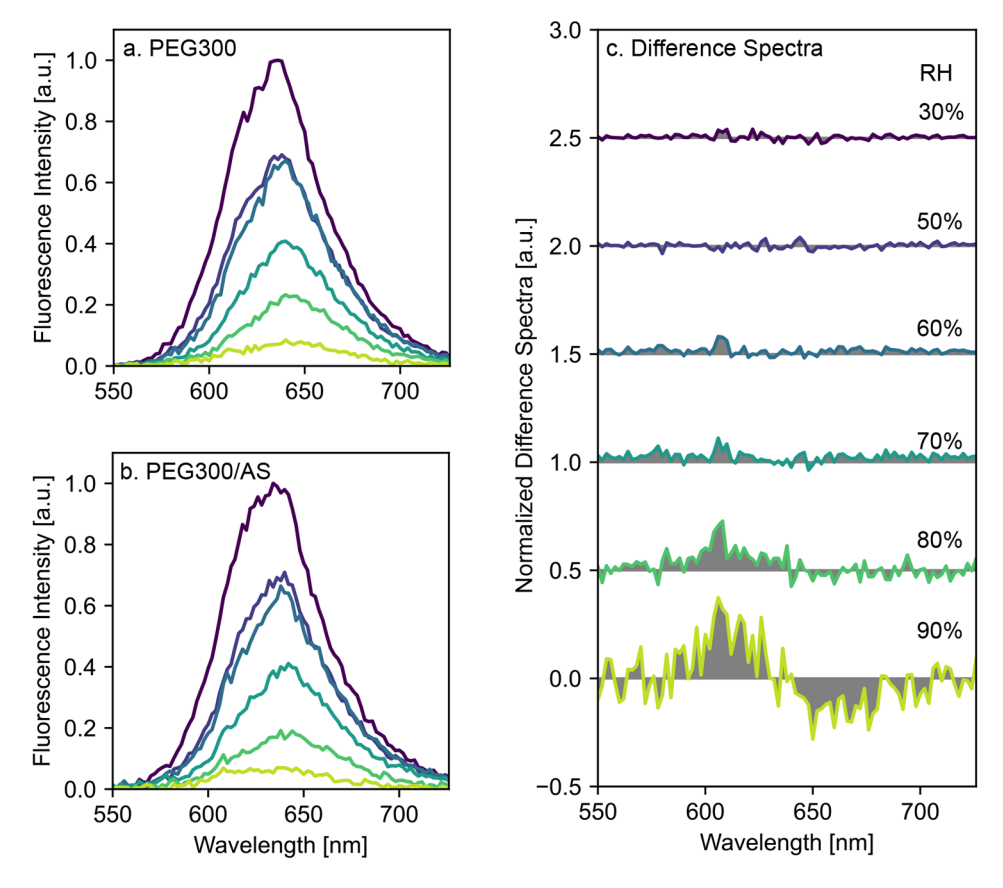


Figure 4. Aerosol fluorescence spectra as a function of RH for (a) Nile Red in PEG300 particles and (b) Nile Red in mixed particles of PEG300 and ammonium sulfate (2:1 mass ratio). Each spectrum is normalized such that the experimental conditions producing the largest signal intensity has a fluorescence intensity of 1 au. (c) Difference spectra between PEG300/AS and PEG300 particles. The difference spectra were calculated from the averages of three individual spectra like those shown in panels a and b. The legend for RH is shown in panel c. The mass ratio between Nile Red and PEG300 was 0.1%. The volume geometric mean diameter of the particles was 168 ± 5 nm (one standard deviation) at 30% RH, and the particle mass concentration was $750 \pm 10 \ \mu g \ m^{-3}$ (Table S1).

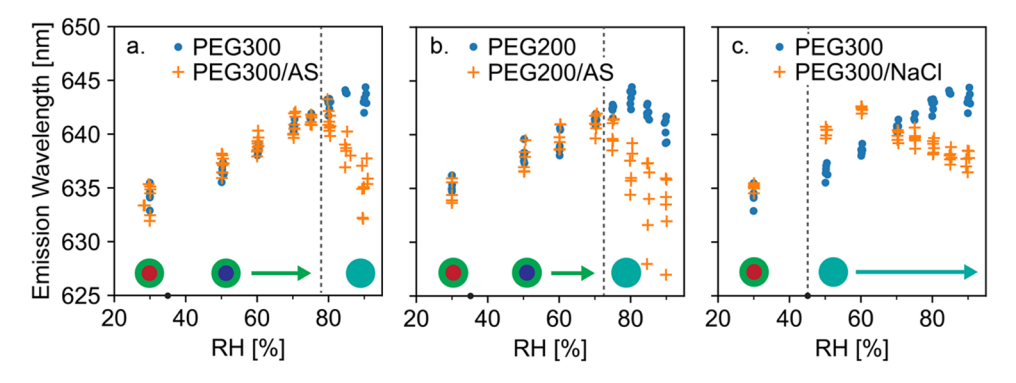


Figure 5. Wavelength of the maximum emission of aerosol fluorescence for Nile Red in (a) PEG300 and PEG300/AS particles, (b) PEG200 and PEG200/AS particles, and (c) PEG300 and PEG300/NaCl particles. Results are shown as a function of RH. Emission maxima were obtained by Gaussian fits to the individual spectra like those shown in Figure 4a,b. The dashed line delineates high and low RH regimes (see main text), and the particle morphologies of these regimes are represented by cartoons along the bottom. Black dots on the abscissa indicate the efflorescence relative humidity of the pure aqueous salts (35% for AS and 45% for NaCl). ¹⁴

that the local chemical environment around NR in the mixed PEG300/AS particles was similar to that in pure PEG particles. This agreement suggests that the mixed particles were phase separated (cases 1a and 1b, Figure 2). Plausibly, the particles represent case 1a of LLPS from 40% to 75% and case 1b of a solid core at 30% RH, given the efflorescence RH of 35% for pure ammonium sulfate. Dissolved impurities such as organic molecules tend to reduce ERH values compared to pure

inorganic components. Therefore, provided that the RH is above the efflorescence RH of the pure aqueous salts, case 1a (LLPS) can be inferred.

For 80% RH and above, Figure 5a shows that the $\lambda_{\rm max}$ values of the mixed particles blue-shifted relative to the reference case. The spectral shift indicates a substantial alteration of the local environment experienced by NR. The probe molecule interacted with water and salt ions under these conditions,

and a morphology of a single-phase mixed particle is implicated (case 2, Figure 2). The foregoing interpretation of cases 1a, 1b, and 2 from 30% to 90% RH is summarized in cartoon form along the bottom of Figure 5a.

3.2.3. Mixed PEG200/AS and Mixed PEG300/NaCl Aerosol Particles. The NR fluorescence behavior as a function of RH is summarized in Figure 5b for pure PEG200 aerosol particles (serving as the source of reference spectra) compared to mixed PEG200/AS aerosol particles. For the reference spectra, $\lambda_{\rm max}$ steadily red-shifted by 9 nm from 30% to 80% RH, in agreement with the behavior of pure PEG300 aerosol particles (Figure 5a). Above 80% RH, however, $\lambda_{\rm max}$ blue-shifted more strongly by up to 4 nm at 90% RH for PEG200 particles. The divergence of $\lambda_{\rm max}$ for the mixed particles from $\lambda_{\rm max}$ of the reference spectra begins above 70% RH. The implication is that LLPS occurred at a SRH between 70% and 75% RH. For comparison, this SRH range is 5% lower than that of the PEG300/AS aerosol particles.

The fluorescence behavior as a function of RH is summarized in Figure 5c for pure PEG300 aerosol particles, serving as reference spectra (same data as shown in Figure 5a) and mixed PEG300/NaCl aerosol particles. For spectra of the mixed particles compared to the reference spectra, the $\lambda_{\rm max}$ values converge at 30% RH and diverge from 50% to 90% RH. An effloresced particle type at 30% RH (case 1b, Figure 2) and homogeneous single-phase particles (case 2, Figure 2) from 50% to 90% RH can explain these observations.

3.3. Comparison to the Literature. The introduced F-AFT has several limitations and capabilities compared to other LLPS-sensitive techniques. In the category of the former, unlike optical microscopy of deposited particles⁴¹ or some Raman spectroscopy-based techniques applied to trapped particles, ⁴⁵ F-AFT as applied herein does not distinguish particle shape or internal morphology, such as core-shell versus partially engulfed particles. The signal is also integrative across a particle population, meaning that any heterogeneity of particle types in a test population is not resolved and, instead, an average behavior is observed. In addition, the time scale of the F-AFT experiments is limited by use of a continuous flow apparatus. For the F-AFT implemented here, between RH conditioning and fluorescence examination, the characteristic time was 5 s. In contrast, a collection of deposited particles or a trapped particle can be exposed to environmental conditions continuously for days while being observed throughout this period. A time scale limitation may be problematic for particle types and conditions that have long gas-particle equilibration times or LLPS nucleation times, whether due to low temperature, high viscosity, or other factors.

An important comparative positive capability is that the F-AFT can study submicron particles in aerosol form and can do so with minimal sample preparation or perturbation. For some particle types and conditions, an aerosol particle can differ from deposited or captured particles in ways that affect SRH and LLPS. The F-AFT is also a continuous, nondestructive online measurement. As such, it can be combined in series or in parallel with other standard online aerosol analytical techniques, such as mass spectrometry or chromatography. The F-AFT can be used to monitor the particle phase state in real time in response to dynamically changing gas compositions or other environmental parameters.

The qualitative LLPS behavior across the different particle systems studied herein by the F-AFT is similar to that reported in the literature for optical microscopy of deposited supermicron particles. Neither technique observed LLPS in PEG300/NaCl

particles to as low as the efflorescence RH (45%).²³ Both techniques observed LLPS in PEG300/AS and PEG200/AS particles, and the SRH for PEG300/AS particles was greater than that for PEG200/AS particles.²³ The difference in SRH may be more influenced by the different oxygen-to-carbon ratios of PEG300 and PEG200, 0.58 and 0.63, respectively, than by changes in molecular weight.⁶⁴

There are some differences in the quantitative results between the two techniques. For the PEG300/AS particles, the SRH was between 75% and 80% RH for submicron aerosol particles in the F-AFT whereas it was reported as 86.7 \pm 2.8% RH for deposited supermicron particles studied by optical microscopy. For the PEG200/AS particles, the SRH values were 70–75% RH in the present study and reported as 79.8 \pm 4.1% for optical microscopy. The difference in SRH between the two sets of studies appears greater than can be explained by experimental uncertainty, including RH calibration, for the different techniques. Results from cryo-TEM of submicron particles likewise indicated lower SRH values than previously observed for deposited supermicron particles by optical microscopy. 49

The explanation for a difference in the SRH of more than 5% RH among the studies could be related to particle size, the presence of the substrate, observation time, or some combination of these factors. Multiple thermodynamic and kinetic effects can influence the SRH of liquid-liquid phase separation. Once the free energy change is favorable for LLPS, phase separation occurs either by nucleation and growth or by spinodal decomposition.⁴³ Nucleation and growth requires crossing an activation barrier and thus can create kinetic limitations to phase separation when it is otherwise thermodynamically favored. 52 The probability for the occurrence of one critical event of nucleation and growth scales with greater supersaturations (i.e., lower RH), larger volumes, longer observation periods, and possible interactions with a substrate, such as heterogeneous nucleation. 65 The last three factors favor LLPS at a higher SRH for deposited supermicron particles compared to suspended submicron aerosol particles. A size dependence for the SRH of LLPS even at slow drying rates could further suggest that thermodynamic factors related to the surface-to-volume ratio may also be important.

4. CONCLUSIONS

Liquid-liquid phase separation in mixed organic/inorganic submicron particles was studied through fluorescence probe spectroscopy in an aerosol flow tube. The probe molecule Nile Red was incorporated into the mixed systems (specifically, PEG/AS and PEG/NaCl), and the separation relative humidity for LLPS was determined for each. The SRH values observed for the suspended submicron aerosol particles were lower by >5% RH compared to previous reports for deposited supermicron particles, and this finding motivates additional future investigations to confirm and further quantify the differences and pinpoint possible explanations. More broadly, in future studies the F-AFT approach might use probe molecules other than Nile Red, such as pH-sensitive dyes⁶⁶ or viscosity-sensitive molecular rotors, 67 to probe additional properties of submicron aerosol particles. Such an approach has been used to probe viscosity in supermicron particles through fluorescence lifetime imaging microscopy. 68-70 Like LLPS, pH and viscosity are recognized as difficult yet important values to obtain in an in situ manner for aerosol particles. 6,7,71-73

In outlook, the F-AFT approach can be applied to study atmospherically relevant aerosol systems, including those composed of semivolatile submicron particles. These particles have nonfixed chemical compositions in dynamic exchange with the gas phase, such as inorganic nitrate and chloride salts as well as complex mixtures of semivolatile organic compounds. In situ aerosol techniques, like the F-AFT, are especially indicated for studies of these types of semivolatile systems. Additional development of a methodology to volatilize probe molecules and condense them onto pre-existing particles could allow F-AFT studies for aerosol particles sampled directly from the ambient environment. As a point of comparison, single-particle fluorescence of primarily supermicron aerosol particles upon excitation with UV wavelengths is widely used for characterizing number concentrations of biologically viable aerosol particles. 74-76 The F-AFT described in this paper can be upgraded for increased sensitivity by incorporation of a more powerful excitation laser, improved collection optics, and a more sensitive detector. These upgrades should allow study of size-selected monodisperse particle populations in the laboratory (this work is presently under way by the authors) as well as operation at the lower mass concentrations characteristic of most real-world atmospheric conditions.

ASSOCIATED CONTENT

Supporting Information

The Supporting Information is available free of charge at https://pubs.acs.org/doi/10.1021/acsearthspace-chem.1c00061.

Particle size distribution statistics (Table S1), fluorescence spectra of Nile Red in bulk solution (Figure S1), and fluorescence emission maxima and intensities for Nile Red in PEG 300 particles as a function of water mass fraction (Figure S2) (PDF)

AUTHOR INFORMATION

Corresponding Author

Scot T. Martin — School of Engineering and Applied Sciences & Department of Earth and Planetary Sciences, Harvard University, Cambridge, Massachusetts 02138, United States; orcid.org/0000-0002-8996-7554; Email: scot_martin@harvard.edu; http://martin.seas.harvard.edu/

Authors

Paul E. Ohno – School of Engineering and Applied Sciences & Department of Earth and Planetary Sciences, Harvard University, Cambridge, Massachusetts 02138, United States; Harvard University Center for the Environment, Cambridge, Massachusetts 02138, United States; orcid.org/0000-0003-4192-1888

Yiming Qin — School of Engineering and Applied Sciences & Department of Earth and Planetary Sciences, Harvard University, Cambridge, Massachusetts 02138, United States; orcid.org/0000-0002-1552-5139

Jianhuai Ye — School of Engineering and Applied Sciences & Department of Earth and Planetary Sciences, Harvard University, Cambridge, Massachusetts 02138, United States; orcid.org/0000-0002-9063-3260

Junfeng Wang — School of Engineering and Applied Sciences & Department of Earth and Planetary Sciences, Harvard University, Cambridge, Massachusetts 02138, United States; orcid.org/0000-0001-6215-1953

Allan K. Bertram — Department of Chemistry, University of British Columbia, Vancouver, British Columbia V6T 1Z1, Canada; orcid.org/0000-0002-5621-2323

Complete contact information is available at: https://pubs.acs.org/10.1021/acsearthspacechem.1c00061

Notes

The authors declare no competing financial interest. The underlying data from the figures including fluorescence spectra, fitted emission maxima and associated RH values, and particle size distributions are available at 10.7910/DVN/CQI09M.

ACKNOWLEDGMENTS

This work was funded in part by Environmental Chemical Sciences of the Division of Chemistry of the U.S. National Science Foundation (Grant ECS-2003368). P.E.O. acknowledges support from the Schmidt Science Fellowship in Partnership with the Rhodes Trust. P.E.O. also acknowledges support from the Harvard University Center for the Environment through the Environmental Fellows Program.

REFERENCES

- (1) Fuzzi, S.; Baltensperger, U.; Carslaw, K.; Decesari, S.; Denier van der Gon, H.; Facchini, M. C.; Fowler, D.; Koren, I.; Langford, B.; Lohmann, U.; Nemitz, E.; Pandis, S.; Riipinen, I.; Rudich, Y.; Schaap, M.; Slowik, J. G.; Spracklen, D. V.; Vignati, E.; Wild, M.; Williams, M.; Gilardoni, S. Particulate Matter, Air Quality and Climate: Lessons Learned and Future Needs. *Atmos. Chem. Phys.* **2015**, *15*, 8217–8299. (2) Fan, J.; Wang, Y.; Rosenfeld, D.; Liu, X. Review of Aerosol—Cloud Interactions: Mechanisms, Significance, and Challenges. *J. Atmos. Sci.* **2016**, *73*, 4221–4252.
- (3) Hallquist, M.; Wenger, J. C.; Baltensperger, U.; Rudich, Y.; Simpson, D.; Claeys, M.; Dommen, J.; Donahue, N. M.; George, C.; Goldstein, A. H.; Hamilton, J. F.; Herrmann, H.; Hoffmann, T.; Iinuma, Y.; Jang, M.; Jenkin, M. E.; Jimenez, J. L.; Kiendler-Scharr, A.; Maenhaut, W.; McFiggans, G.; Mentel, T. F.; Monod, A.; Prévôt, A. S. H.; Seinfeld, J. H.; Surratt, J. D.; Szmigielski, R.; Wildt, J. The Formation, Properties and Impact of Secondary Organic Aerosol: Current and Emerging Issues. Atmos. Chem. Phys. 2009, 9, 5155–5236.
- (4) Pöschl, U.; Shiraiwa, M. Multiphase Chemistry at the Atmosphere–Biosphere Interface Influencing Climate and Public Health in the Anthropocene. *Chem. Rev.* **2015**, 115, 4440–4475.
- (5) Shrivastava, M.; Cappa, C. D.; Fan, J.; Goldstein, A. H.; Guenther, A. B.; Jimenez, J. L.; Kuang, C.; Laskin, A.; Martin, S. T.; Ng, N. L.; Petaja, T.; Pierce, J. R.; Rasch, P. J.; Roldin, P.; Seinfeld, J. H.; Shilling, J.; Smith, J. N.; Thornton, J. A.; Volkamer, R.; Wang, J.; Worsnop, D. R.; Zaveri, R. A.; Zelenyuk, A.; Zhang, Q. Recent Advances in Understanding Secondary Organic Aerosol: Implications for Global Climate Forcing. *Rev. Geophys.* 2017, 55, 509–559.
- (6) Reid, J. P.; Bertram, A. K.; Topping, D. O.; Laskin, A.; Martin, S. T.; Petters, M. D.; Pope, F. D.; Rovelli, G. The Viscosity of Atmospherically Relevant Organic Particles. *Nat. Commun.* **2018**, *9*, 956.
- (7) Pye, H. O. T.; Nenes, A.; Alexander, B.; Ault, A. P.; Barth, M. C.; Clegg, S. L.; Collett, J. L., Jr.; Fahey, K. M.; Hennigan, C. J.; Herrmann, H.; Kanakidou, M.; Kelly, J. T.; Ku, I. T.; McNeill, V. F.; Riemer, N.; Schaefer, T.; Shi, G.; Tilgner, A.; Walker, J. T.; Wang, T.; Weber, R.; Xing, J.; Zaveri, R. A.; Zuend, A. The Acidity of Atmospheric Particles and Clouds. *Atmos. Chem. Phys.* **2020**, *20*, 4809–4888.
- (8) Pankow, J. F. Gas/Particle Partitioning of Neutral and Ionizing Compounds to Single and Multi-Phase Aerosol Particles. 1. Unified Modeling Framework. *Atmos. Environ.* **2003**, *37*, 3323–3333.
- (9) Erdakos, G. B.; Pankow, J. F. Gas/Particle Partitioning of Neutral and Ionizing Compounds to Single- and Multi-Phase Aerosol Particles. 2. Phase Separation in Liquid Particulate Matter Containing Both Polar

- and Low-Polarity Organic Compounds. Atmos. Environ. 2004, 38, 1005-1013.
- (10) Marcolli, C.; Krieger, U. K. Phase Changes During Hygroscopic Cycles of Mixed Organic/Inorganic Model Systems of Tropospheric Aerosols. *J. Phys. Chem. A* **2006**, *110*, 1881–1893.
- (11) Krieger, U. K.; Marcolli, C.; Reid, J. P. Exploring the Complexity of Aerosol Particle Properties and Processes Using Single Particle Techniques. *Chem. Soc. Rev.* **2012**, *41*, 6631–6662.
- (12) You, Y.; Smith, M. L.; Song, M.; Martin, S. T.; Bertram, A. K. Liquid—Liquid Phase Separation in Atmospherically Relevant Particles Consisting of Organic Species and Inorganic Salts. *Int. Rev. Phys. Chem.* **2014**, 33, 43–77.
- (13) Freedman, M. A. Phase Separation in Organic Aerosol. Chem. Soc. Rev. 2017, 46, 7694–7705.
- (14) Martin, S. T. Phase Transitions of Aqueous Atmospheric Particles. *Chem. Rev.* **2000**, *100*, 3403–3454.
- (15) Seinfeld, J. H.; Pandis, S. N. Atmospheric Chemistry and Physics: From Air Pollution to Climate Change; John Wiley & Sons: Hoboken, NJ, 2016
- (16) Wang, J.; Hoffmann, A. A.; Park, R. J.; Jacob, D. J.; Martin, S. T. Global Distribution of Solid and Aqueous Sulfate Aerosols: Effect of the Hysteresis of Particle Phase Transitions. *J. Geophys. Res.* **2008**, *113*, D11206
- (17) Chang, E. I.; Pankow, J. F. Prediction of Activity Coefficients in Liquid Aerosol Particles Containing Organic Compounds, Dissolved Inorganic Salts, and Water—Part 2: Consideration of Phase Separation Effects by an X-UNIFAC Model. *Atmos. Environ.* **2006**, *40*, 6422–6436.
- (18) Ciobanu, V. G.; Marcolli, C.; Krieger, U. K.; Weers, U.; Peter, T. Liquid-Liquid Phase Separation in Mixed Organic/Inorganic Aerosol Particles. *J. Phys. Chem. A* **2009**, *113*, 10966–10978.
- (19) Zuend, A.; Marcolli, C.; Peter, T.; Seinfeld, J. H. Computation of Liquid-Liquid Equilibria and Phase Stabilities: Implications for RH-Dependent Gas/Particle Partitioning of Organic-Inorganic Aerosols. *Atmos. Chem. Phys.* **2010**, *10*, 7795–7820.
- (20) Song, M.; Marcolli, C.; Krieger, U. K.; Zuend, A.; Peter, T. Liquid-Liquid Phase Separation in Aerosol Particles: Dependence on O:C, Organic Functionalities, and Compositional Complexity. *Geophys. Res. Lett.* **2012**, *39*, L19801.
- (21) Bertram, A. K.; Martin, S. T.; Hanna, S. J.; Smith, M. L.; Bodsworth, A.; Chen, Q.; Kuwata, M.; Liu, A.; You, Y.; Zorn, S. R. Predicting the Relative Humidities of Liquid-Liquid Phase Separation, Efflorescence, and Deliquescence of Mixed Particles of Ammonium Sulfate, Organic Material, and Water Using the Organic-to-Sulfate Mass Ratio of the Particle and the Oxygen-to-Carbon Elemental Ratio of the Organic Component. *Atmos. Chem. Phys.* **2011**, *11*, 10995–11006.
- (22) You, Y.; Renbaum-Wolff, L.; Carreras-Sospedra, M.; Hanna, S. J.; Hiranuma, N.; Kamal, S.; Smith, M. L.; Zhang, X.; Weber, R. J.; Shilling, J. E.; Dabdub, D.; Martin, S. T.; Bertram, A. K. Images Reveal That Atmospheric Particles Can Undergo Liquid—Liquid Phase Separations. *Proc. Natl. Acad. Sci. U. S. A.* **2012**, *109*, 13188.
- (23) You, Y.; Renbaum-Wolff, L.; Bertram, A. K. Liquid—Liquid Phase Separation in Particles Containing Organics Mixed with Ammonium Sulfate, Ammonium Bisulfate, Ammonium Nitrate or Sodium Chloride. *Atmos. Chem. Phys.* **2013**, *13*, 11723—11734.
- (24) Veghte, D. P.; Altaf, M. B.; Freedman, M. A. Size Dependence of the Structure of Organic Aerosol. *J. Am. Chem. Soc.* **2013**, *135*, 16046–16049.
- (25) Losey, D. J.; Parker, R. G.; Freedman, M. A. pH Dependence of Liquid–Liquid Phase Separation in Organic Aerosol. *J. Phys. Chem. Lett.* **2016**, *7*, 3861–3865.
- (26) Kucinski, T. M.; Dawson, J. N.; Freedman, M. A. Size-Dependent Liquid—Liquid Phase Separation in Atmospherically Relevant Complex Systems. *J. Phys. Chem. Lett.* **2019**, *10*, 6915—6920.
- (27) Zuend, A.; Seinfeld, J. H. Modeling the Gas-Particle Partitioning of Secondary Organic Aerosol: The Importance of Liquid-Liquid Phase Separation. *Atmos. Chem. Phys.* **2012**, *12*, 3857–3882.
- (28) Kwamena, N. O. A.; Staikova, M. G.; Donaldson, D. J.; George, I. J.; Abbatt, J. P. D. Role of the Aerosol Substrate in the Heterogeneous

- Ozonation Reactions of Surface-Bound Pahs. J. Phys. Chem. A 2007, 111, 11050-11058.
- (29) Sage, A. M.; Weitkamp, E. A.; Robinson, A. L.; Donahue, N. M. Reactivity of Oleic Acid in Organic Particles: Changes in Oxidant Uptake and Reaction Stoichiometry with Particle Oxidation. *Phys. Chem. Chem. Phys.* **2009**, *11*, 7951–7962.
- (30) Reid, J. P.; Dennis-Smither, B. J.; Kwamena, N.-O. A.; Miles, R. E. H.; Hanford, K. L.; Homer, C. J. The Morphology of Aerosol Particles Consisting of Hydrophobic and Hydrophilic Phases: Hydrocarbons, Alcohols and Fatty Acids as the Hydrophobic Component. *Phys. Chem. Phys.* **2011**, *13*, 15559–15572.
- (31) Brunamonti, S.; Krieger, U. K.; Marcolli, C.; Peter, T. Redistribution of Black Carbon in Aerosol Particles Undergoing Liquid-Liquid Phase Separation. *Geophys. Res. Lett.* **2015**, 42, 2532–2539
- (32) Fard, M. M.; Krieger, U. K.; Peter, T. Shortwave Radiative Impact of Liquid—Liquid Phase Separation in Brown Carbon Aerosols. *Atmos. Chem. Phys.* **2018**, *18*, 13511—13530.
- (33) Shiraiwa, M.; Zuend, A.; Bertram, A. K.; Seinfeld, J. H. Gas—Particle Partitioning of Atmospheric Aerosols: Interplay of Physical State, Non-Ideal Mixing and Morphology. *Phys. Chem. Chem. Phys.* **2013**, *15*, 11441–11453.
- (34) Topping, D.; Barley, M.; McFiggans, G. Including Phase Separation in a Unified Model to Calculate Partitioning of Vapours to Mixed Inorganic—Organic Aerosol Particles. *Faraday Discuss.* **2013**, 165, 273—288.
- (35) Renbaum-Wolff, L.; Song, M.; Marcolli, C.; Zhang, Y.; Liu, P. F.; Grayson, J. W.; Geiger, F. M.; Martin, S. T.; Bertram, A. K. Observations and Implications of Liquid–Liquid Phase Separation at High Relative Humidities in Secondary Organic Material Produced by A-Pinene Ozonolysis without Inorganic Salts. *Atmos. Chem. Phys.* **2016**, *16*, 7969–7979.
- (36) Ovadnevaite, J.; Zuend, A.; Laaksonen, A.; Sanchez, K. J.; Roberts, G.; Ceburnis, D.; Decesari, S.; Rinaldi, M.; Hodas, N.; Facchini, M. C.; Seinfeld, J. H.; O' Dowd, C. Surface Tension Prevails over Solute Effect in Organic-Influenced Cloud Droplet Activation. *Nature* **2017**, *546*, 637–641.
- (37) Rastak, N.; Pajunoja, A.; Acosta Navarro, J. C.; Ma, J.; Song, M.; Partridge, D. G.; Kirkevåg, A.; Leong, Y.; Hu, W. W.; Taylor, N. F.; Lambe, A.; Cerully, K.; Bougiatioti, A.; Liu, P.; Krejci, R.; Petäjä, T.; Percival, C.; Davidovits, P.; Worsnop, D. R.; Ekman, A. M. L.; Nenes, A.; Martin, S.; Jimenez, J. L.; Collins, D. R.; Topping, D. O.; Bertram, A. K.; Zuend, A.; Virtanen, A.; Riipinen, I. Microphysical Explanation of the RH-Dependent Water Affinity of Biogenic Organic Aerosol and Its Importance for Climate. *Geophys. Res. Lett.* 2017, 44, 5167–5177.
- (38) Liu, P.; Song, M.; Zhao, T.; Gunthe, S. S.; Ham, S.; He, Y.; Qin, Y. M.; Gong, Z.; Amorim, J. C.; Bertram, A. K.; Martin, S. T. Resolving the Mechanisms of Hygroscopic Growth and Cloud Condensation Nuclei Activity for Organic Particulate Matter. *Nat. Commun.* **2018**, *9*, 4076.
- (39) Altaf, M. B.; Dutcher, D. D.; Raymond, T. M.; Freedman, M. A. Effect of Particle Morphology on Cloud Condensation Nuclei Activity. *ACS Earth Space Chem.* **2018**, *2*, 634–639.
- (40) Ault, A. P.; Axson, J. L. Atmospheric Aerosol Chemistry: Spectroscopic and Microscopic Advances. *Anal. Chem.* **2017**, *89*, 430–452.
- (41) Song, M.; Marcolli, C.; Krieger, U. K.; Zuend, A.; Peter, T. Liquid-Liquid Phase Separation and Morphology of Internally Mixed Dicarboxylic Acids/Ammonium Sulfate/Water Particles. *Atmos. Chem. Phys.* **2012**, *12*, 2691–2712.
- (42) O'Brien, R. E.; Wang, B.; Kelly, S. T.; Lundt, N.; You, Y.; Bertram, A. K.; Leone, S. R.; Laskin, A.; Gilles, M. K. Liquid–Liquid Phase Separation in Aerosol Particles: Imaging at the Nanometer Scale. *Environ. Sci. Technol.* **2015**, *49*, 4995–5002.
- (43) Freedman, M. A. Liquid-Liquid Phase Separation in Supermicrometer and Submicrometer Aerosol Particles. *Acc. Chem. Res.* **2020**, 53, 1102–1110.
- (44) Lee, A. K. Y.; Ling, T. Y.; Chan, C. K. Understanding Hygroscopic Growth and Phase Transformation of Aerosols Using

- Single Particle Raman Spectroscopy in an Electrodynamic Balance. *Faraday Discuss.* **2008**, *137*, 245–263.
- (45) Sullivan, R. C.; Boyer-Chelmo, H.; Gorkowski, K.; Beydoun, H. Aerosol Optical Tweezers Elucidate the Chemistry, Acidity, Phase Separations, and Morphology of Atmospheric Microdroplets. *Acc. Chem. Res.* **2020**, *53*, 2498–2509.
- (46) Gorkowski, K.; Donahue, N. M.; Sullivan, R. C. Emulsified and Liquid—Liquid Phase-Separated States of A-Pinene Secondary Organic Aerosol Determined Using Aerosol Optical Tweezers. *Environ. Sci. Technol.* **2017**, *51*, 12154—12163.
- (47) Gorkowski, K.; Donahue, N. M.; Sullivan, R. C. Aerosol Optical Tweezers Constrain the Morphology Evolution of Liquid-Liquid Phase-Separated Atmospheric Particles. *Chem.* **2020**, *6*, 204–220.
- (48) Altaf, M. B.; Freedman, M. A. Effect of Drying Rate on Aerosol Particle Morphology. J. Phys. Chem. Lett. 2017, 8, 3613–3618.
- (49) Kucinski, T. M.; Ott, E.-J. E.; Freedman, M. A. Flash Freeze Flow Tube to Vitrify Aerosol Particles at Fixed Relative Humidity Values. *Anal. Chem.* **2020**, 92, 5207–5213.
- (50) Klymchenko, A. S. Solvatochromic and Fluorogenic Dyes as Environment-Sensitive Probes: Design and Biological Applications. *Acc. Chem. Res.* **2017**, *50*, 366–375.
- (51) Bouzidi, H.; Zuend, A.; Ondráček, J.; Schwarz, J.; Ždímal, V. Hygroscopic Behavior of Inorganic—Organic Aerosol Systems Including Ammonium Sulfate, Dicarboxylic Acids, and Oligomer. *Atmos. Environ.* **2020**, 229, 117481.
- (52) Altaf, M. B.; Zuend, A.; Freedman, M. A. Role of Nucleation Mechanism on the Size Dependent Morphology of Organic Aerosol. *Chem. Commun.* **2016**, *52*, 9220–9223.
- (53) Wang, S. C.; Flagan, R. C. Scanning Electrical Mobility Spectrometer. *Aerosol Sci. Technol.* **1990**, *13*, 230–240.
- (54) Biskos, G.; Paulsen, D.; Russell, L. M.; Buseck, P. R.; Martin, S. T. Prompt Deliquescence and Efflorescence of Aerosol Nanoparticles. *Atmos. Chem. Phys.* **2006**, *6*, 4633–4642.
- (55) Greenspan, P.; Mayer, E. P.; Fowler, S. D. Nile Red: A Selective Fluorescent Stain for Intracellular Lipid Droplets. *J. Cell Biol.* **1985**, *100*, 965–973
- (56) Greenspan, P.; Fowler, S. D. Spectrofluorometric Studies of the Lipid Probe, Nile Red. *J. Lipid Res.* **1985**, 26, 781–9.
- (57) Lee, H. J.; Laskin, A.; Laskin, J.; Nizkorodov, S. A. Excitation— Emission Spectra and Fluorescence Quantum Yields for Fresh and Aged Biogenic Secondary Organic Aerosols. *Environ. Sci. Technol.* **2013**, 47, 5763—5770.
- (58) Sackett, D. L.; Wolff, J. Nile Red as a Polarity-Sensitive Fluorescent Probe of Hydrophobic Protein Surfaces. *Anal. Biochem.* **1987**, *167*, 228–234.
- (59) Lakowicz, J. R. Principles of Fluorescence Spectroscopy; Springer: New York, 2006.
- (60) Valeur, B. Molecular Fluorescence: Principles and Applications; Wiley-VCH Verlag GmbH & Co. KGaA: Weinheim, Germany, 2013.
- (61) Ray, A.; Das, S.; Chattopadhyay, N. Aggregation of Nile Red in Water: Prevention through Encapsulation in B-Cyclodextrin. *ACS Omega* **2019**, *4*, 15–24.
- (62) Kurniasih, I. N.; Liang, H.; Mohr, P. C.; Khot, G.; Rabe, J. P.; Mohr, A. Nile Red Dye in Aqueous Surfactant and Micellar Solution. *Langmuir* **2015**, *31*, 2639–2648.
- (63) Dutta, A. K.; Kamada, K.; Ohta, K. Spectroscopic Studies of Nile Red in Organic Solvents and Polymers. *J. Photochem. Photobiol., A* **1996**, 93, 57–64.
- (64) You, Y.; Bertram, A. K. Effects of Molecular Weight and Temperature on Liquid-Liquid Phase Separation in Particles Containing Organic Species and Inorganic Salts. *Atmos. Chem. Phys.* **2015**, *15*, 1351–1365.
- (65) Hung, H.-M.; Martin, S. T. Apparent Freezing Temperatures Modeled for Several Experimental Apparatus. *J. Geophys. Res. Atmos.* **2001**, *106*, 20379–20394.
- (66) Steinegger, A.; Wolfbeis, O. S.; Borisov, S. M. Optical Sensing and Imaging of pH Values: Spectroscopies, Materials, and Applications. *Chem. Rev.* **2020**, *120*, 12357–12489.

- (67) Hosny, N. A.; Fitzgerald, C.; Tong, C.; Kalberer, M.; Kuimova, M. K.; Pope, F. D. Fluorescent Lifetime Imaging of Atmospheric Aerosols: A Direct Probe of Aerosol Viscosity. *Faraday Discuss.* **2013**, 165, 343–356.
- (68) Hosny, N. A.; Fitzgerald, C.; Vyšniauskas, A.; Athanasiadis, A.; Berkemeier, T.; Uygur, N.; Pöschl, U.; Shiraiwa, M.; Kalberer, M.; Pope, F. D.; Kuimova, M. K. Direct Imaging of Changes in Aerosol Particle Viscosity Upon Hydration and Chemical Aging. *Chem. Sci.* **2016**, *7*, 1357–1367.
- (69) Fitzgerald, C.; Hosny, N. A.; Tong, H.; Seville, P. C.; Gallimore, P. J.; Davidson, N. M.; Athanasiadis, A.; Botchway, S. W.; Ward, A. D.; Kalberer, M.; Kuimova, M. K.; Pope, F. D. Fluorescence Lifetime Imaging of Optically Levitated Aerosol: A Technique to Quantitatively Map the Viscosity of Suspended Aerosol Particles. *Phys. Chem. Chem. Phys.* **2016**, *18*, 21710–21719.
- (70) Athanasiadis, A.; Fitzgerald, C.; Davidson, N. M.; Giorio, C.; Botchway, S. W.; Ward, A. D.; Kalberer, M.; Pope, F. D.; Kuimova, M. K. Dynamic Viscosity Mapping of the Oxidation of Squalene Aerosol Particles. *Phys. Chem. Chem. Phys.* **2016**, *18*, 30385–30393.
- (71) Zhang, Y.; Chen, Y.; Lei, Z.; Olson, N. E.; Riva, M.; Koss, A. R.; Zhang, Z.; Gold, A.; Jayne, J. T.; Worsnop, D. R.; Onasch, T. B.; Kroll, J. H.; Turpin, B. J.; Ault, A. P.; Surratt, J. D. Joint Impacts of Acidity and Viscosity on the Formation of Secondary Organic Aerosol from Isoprene Epoxydiols (IEPOX) in Phase Separated Particles. ACS Earth Space Chem. 2019, 3, 2646.
- (72) Ault, A. P. Aerosol Acidity: Novel Measurements and Implications for Atmospheric Chemistry. *Acc. Chem. Res.* **2020**, *53*, 1703–1714.
- (73) Schmedding, R.; Rasool, Q. Z.; Zhang, Y.; Pye, H. O. T.; Zhang, H.; Chen, Y.; Surratt, J. D.; Lopez-Hilfiker, F. D.; Thornton, J. A.; Goldstein, A. H.; Vizuete, W. Predicting Secondary Organic Aerosol Phase State and Viscosity and Its Effect on Multiphase Chemistry in a Regional-Scale Air Quality Model. *Atmos. Chem. Phys.* **2020**, 20, 8201–8225.
- (74) Huffman, J. A.; Sinha, B.; Garland, R. M.; Snee-Pollmann, A.; Gunthe, S. S.; Artaxo, P.; Martin, S. T.; Andreae, M. O.; Pöschl, U. Size Distributions and Temporal Variations of Biological Aerosol Particles in the Amazon Rainforest Characterized by Microscopy and Real-Time UV-APS Fluorescence Techniques During Amaze-08. *Atmos. Chem. Phys.* **2012**, *12*, 11997–12019.
- (75) Fennelly, M. J.; Sewell, G.; Prentice, M. B.; O'Connor, D. J.; Sodeau, J. R. Review: The Use of Real-Time Fluorescence Instrumentation to Monitor Ambient Primary Biological Aerosol Particles (PBAP). *Atmosphere* **2018**, *9*, 1.
- (76) Zhang, M.; Klimach, T.; Ma, N.; Könemann, T.; Pöhlker, C.; Wang, Z.; Kuhn, U.; Scheck, N.; Pöschl, U.; Su, H.; Cheng, Y. Size-Resolved Single-Particle Fluorescence Spectrometer for Real-Time Analysis of Bioaerosols: Laboratory Evaluation and Atmospheric Measurements. *Environ. Sci. Technol.* **2019**, *53*, 13257–13264.